Controlling the optical scattering of plasmonic nanoparticles using a thin dielectric layer

A. W. Powell, M. B. Wincott, A. A. R. Watt, H. E. Assender, and J. M. Smith

Citation: J. Appl. Phys. **113**, 184311 (2013); doi: 10.1063/1.4804964
View online: http://dx.doi.org/10.1063/1.4804964
View Table of Contents: http://jap.aip.org/resource/1/JAPIAU/v113/i18
Published by the American Institute of Physics.

JOURNAL OF APPLIED PHYSICS **113**, 184311 (2013)

Controlling the optical scattering of plasmonic nanoparticles using a thin dielectric layer

A. W. Powell,[a] M. B. Wincott, A. A. R. Watt,[b] H. E. Assender,[c] and J. M. Smith[d]
Department of Materials, University of Oxford, Parks Road, Oxford OX1 3PH, United Kingdom

(Received 1 February 2013; accepted 29 April 2013; published online 14 May 2013)

The effect of a thin dielectric film on the plasmonic behaviour of metal nanoparticles (MNPs) above a high refractive index substrate is explored. Using finite-difference time domain simulations, the optical properties of Ag nanoparticles are investigated as a function of film thickness, refractive index, and particle position within the film. We demonstrate that the addition of a film around a MNP at the air interface of a high-index substrate, where $n_{air} < n_{film} < n_{substrate}$, will always increase the fraction of light coupled to the substrate (F_{subs}). It is found that placement within a layer that does not conform to $n_{air} < n_{film} < n_{substrate}$ can lead to reduced enhancements in F_{subs}. The principal application for this work is for light-trapping in thin-film solar cells. We show that the inclusion of a thin film can increase the fraction of radiation coupled into the substrate by up to 30% for solar wavelengths. Additional potential benefits of the film structure, such as greater tunability of scattering resonances, an increase in path length of light in the substrate, and some control over the emission pattern are demonstrated. MNPs in a film are found to produce a more finely structured emission pattern than particles at a simple interface, showing potential for this research to be applied to optical nanoantennae. © *2013 AIP Publishing LLC*.
[http://dx.doi.org/10.1063/1.4804964]

I. INTRODUCTION

Over the past few years, the resonant properties of localised surface plasmons (LSPs) in metal nanoparticles (MNPs) have attracted a rapid growth in interest across a range of fields.[1–3] The large optical cross-sections and scattering efficiencies of LSPs make them an ideal candidate for light-trapping in solar cells,[4] while the strong dependence of their resonant behaviour on the dielectric environment around the particle has enabled many developments in biosensing.[3] Near-field coupling of LSPs to a high-index substrate and between neighboring particles has been effectively utilised to produce unidirectional nanoantennas for single emitters.[5–7]

For thin-film photovoltaic (PV) cells, plasmon-induced scattering from MNPs can be used to trap a large fraction of incident sunlight within a thin active layer. This enables efficient charge extraction without compromising absorption, thus boosting the conversion efficiency of the cell.[8] There are many examples of this method producing significant enhancements in absorption,[9–11] short-circuit current,[12,13] and external quantum efficiency.[14–16] Power conversion efficiency (PCE) enhancements of 23% for amorphous Si[17] and 19% for organic cells[18] have been achieved.

LSPs are coherent oscillations of the free electrons in a MNP, induced by the electric field of incident photons. Depending on the conditions, they can be excited into a single resonant mode of the particle geometry, such as dipole and quadrupole, or a superposition of modes.[19] Each resonance condition is a function of the size, shape, and material of the particle as well as the surrounding environment.[2,20] These excitations can decay radiatively, to produce scattering, or non-radiatively, resulting in absorption. LSPs can produce a significant field enhancement over a cross-section greater than that of the particle itself, allowing MNPs to scatter or absorb incident radiation across a large area.

Whilst there has been much research into the properties of MNPs, a detailed investigation of their scattering behaviour in a thin-film dielectric environment has yet to be undertaken. Previous work has mostly focused on particles at the interface of the semiconducting material with free space, which will rarely be the case in completed devices. Even if the MNPs are placed at the front of a PV cell, before the active region and any other conducting layers, thin-film cells are typically coated in a sub-100 nm protective oxide,[21] which will affect the optical properties. Recent reports have investigated MNPs in other regions of the structure and have demonstrated some potential advantages to utilising the multi-layered structure of the cell.[22–25] However, the emphasis so far has been on bulk effects due to extended MNP arrays, and the manner in which the dielectric environment in thin-films affects MNP behaviour remains to be explored systematically. Recent studies have shown that in the case of a dipolar optical source, placing it in a thin dielectric layer above a high refractive index (RI) substrate can radically alter the emission properties compared to the case of a dipole at a simple interface.[26,27] By tuning the properties of the layer and the position of the emitter, it is possible to enhance the coupling of light into the substrate and to alter the far-field emission pattern.[26] For light scattering from a MNP, behaviour due to the dipolar plasmonic resonance will generally be dominant across most of the solar spectrum.

[a]Electronic mail: alexander.powell@materials.ox.ac.uk
[b]URL: http://www-solar.materials.ox.ac.uk/
[c]URL: http://polymers.materials.ox.ac.uk/
[d]URL: http://www-png.materials.ox.ac.uk

However, contributions from higher order excitations, which have different spatial distributions and loss characteristics can be significant at shorter wavelengths.[12,28,29]

This paper extends the scope of previous research to analyse the scattering properties of a MNP in a thin dielectric film above a high RI substrate. Through simulations using finite-difference time domain (FDTD) software, we investigate how the properties of a thin-film structure affect the MNP scattering cross-section, efficiency of emission into a higher-index substrate, and far-field scattering pattern. We show that the fraction of radiation scattered into the substrate can be significantly enhanced by the addition of the film; light can be scattered to larger angles enhancing path length, and the scattering resonance can be tuned and broadened. These results are highly relevant for use in thin-film photovoltaic cells, but are also of general interest for any application that places MNPs in a planar thin-film environment.

II. SIMULATION

Figure 1 shows the structure used in the simulations. An Ag particle was placed within a thin dielectric film in between two half-spaces; one modelled as a dielectric, the other as free space. The RI of layers was set as $n_{air} = 1$, $n_{film} = 1.5, n_{subs} = 1.8$, corresponding to air, Polyvinyl acetate (PVA), and sapphire layers. These layers also bear much similarity to a P3HT:PCBM, PEDOT:PSS structure seen in many organic photovoltaic (OPV) cells,[30,31] albeit without a front electrical contact. Only single nanoparticles are examined in this report—so grating effects from ordered arrays are not accounted for. However, studies involving single nanoparticles have been shown to be a good approximation for the behaviour of random particle arrays, where MNPs are spaced far enough to be non-interacting.[14] Light is incident from the free space side along the z-axis and is linearly polarised parallel to the *y*-axis.

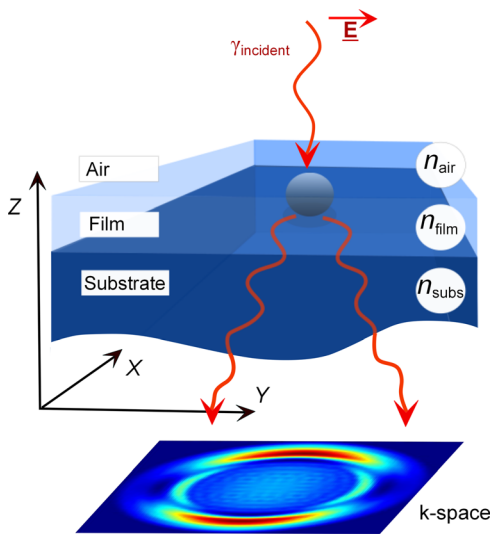

FIG. 1. The geometry to be explored. A scatterer is placed within a thin layer with refractive index n_{film} between an infinitely thick substrate with a refractive index n_{subs} and an upper half-space characterised by n_{air}. The angular scattering of the particle into the substrate is represented as a k-space plot.

Simulations were conducted using Lumerical,[32] an FDTD program which uses Maxwell's equations to calculate numerically the propagation of electromagnetic fields through a defined structure. FDTD simulations offer scope to obtain information about MNPs, which are difficult to determine using numerical models, such as the fraction of light emitted into the substrate across the solar spectrum and the behaviour of higher-order modes. Perfectly matched layer (PML) boundary conditions were chosen at all edges to ensure that no light is reflected back into the simulation region. A Total Field Scattered Field (TFSF) illumination source was used for MNP simulations,[33] which defines a 3D source region with the illumination incident from one plane. The field leaving the region after illumination is measured, and the incident excitation field subtracted, enabling us to measure solely the field contributions due to scattering and absorption from the plasmonic particle. The program also measures the electric field scattered into the substrate or the upper layer and applies a Fourier transform to obtain k-space intensity plots of the angular scattering in each layer.

III. DIPOLES IN THIN LAYERS

The behaviour of dipoles in a multi-layered environment is well known and as the principal excitation in an MNP is generally dipolar, this provides a good starting point for analysing the behaviour of MNP scatterers in a film before moving on to discuss higher order resonances and other effects more specific to plasmonic particles. A model developed by Neyts[34] provides a conceptual understanding of the behaviour of dipoles in multilayered structures.

We consider a purely dipolar emitter in a thin dielectric layer positioned with its centre a distance z_- from the substrate and a distance z_+ from the air interface of the film (Fig. 2(a)). The total film thickness is given as $t = z_+ + z_-$. This will be the notation used throughout this paper, and when discussing spherical particles, z_+, z_- will always be taken from the centre of the particle. A fraction of all emitted radiation will be reflected from either interface as a function of angle and the RI of the layers. Reflected and incident radiation interfere, creating a highly altered emission pattern in the far field when compared to the case of a dipole in free space (Fig. 3). If the dipole is close to an interface (z_+ or z_- is small), it will also emit preferentially into the higher index layer due to its greater optical density of states.[35]

The fraction and angular properties of light emitted into the substrate are determined by two major types of reflective interference in the film: wide-angle interference, between light emitted directly into the substrate and that reflected from the upper interface (Fig. 2(a)), and multi-beam interference, between multiple reflections of light within the layer (Fig. 2(b)). Wide angle interference dominates the emission properties when $n_{subs} > n_{film} > n_{air}$, especially when $n_{film} \approx n_{subs}$, and is a function of z_+. Multi-beam interference is a cavity effect, dependent on the film thickness, t and is the principal mechanism when $n_{film} > n_{subs}, n_{air}$.

With no film present, light emitted at large angles will not enter the substrate and will be lost. By choosing appropriate RI values for the layers, these interference effects can

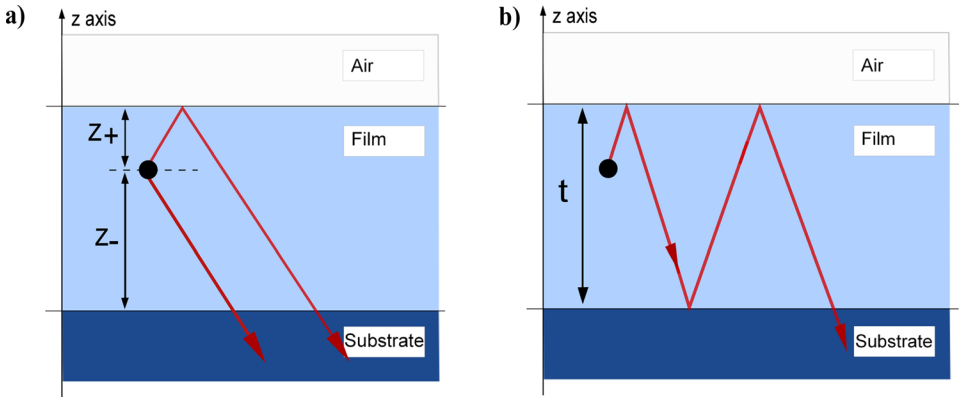

FIG. 2. A dipolar scatterer or emitter is placed within a thin layer with its centre a distance z_- from an infinitely thick substrate and z_+ from an upper half-space. (a) An illustration of wide angle interference for dipolar emitters, which dominates the emission properties when $n_{subs} > n_{film} > n_{air}$. (b) Multiple-beam interference, which dominates when $n_{film} > n_{subs}, n_{air}$.

be manipulated so the film acts as a quasi-waveguide, catching some of this high-angle emission via total-internal reflection and channeling it into the substrate at well-defined angles. Some control over the emission pattern into the substrate can also be achieved by altering the RI and film thickness, and the position of the emitter within the film, as shall be discussed further in Sec. VI.

To highlight the effect the addition of a film has on some of the emission properties of a dipole, Fig. 3 displays the far-field emission patterns in the substrate for a 750 nm dipole source. Figure 3(a) shows the k-space plot for a dipole at the air interface of a high-index substrate with no intermediate film, oriented parallel to the surface. Most of the emitted radiation is directed into the substrate due to its larger refractive index. Figure 3(b) shows the case where the dipole is placed within an intermediate layer with a refractive index, $n_{film} = 1.5$, so $n_{air} < n_{film} < n_{subs}$. The interference created by the layer produces a significantly altered pattern, with less light emitted close to the normal and more at larger angles, which is beneficial for light trapping applications. The difference in behaviour is highlighted in Fig. 3(c), where it is also clear that the addition of the film reduces backscatter—leading here to a 12% increase in the fraction coupled into the substrate at this wavelength.

The dipolar model described here provides a good a conceptual understanding of the effect the film has on a dipole emitter, and is useful for understanding some of the effects that varying the parameters has on particle scattering behaviour. Although FDTD simulations are used to obtain the results throughout this paper, the dipolar picture is useful as a tool to interpret these results.

IV. RESPONSE OF SPHERICAL AND HEMISPHERICAL MNPs TO A THIN FILM

Placing a MNP in a thin film adds an extra parameter alongside particle size and shape, which will affect the resonance conditions of the particle. Figure 4 shows the optical scattering, Q_{scat} and absorption, Q_{abs} cross sections (normalised to the geometric cross-section of the particles) for 150 nm diameter spheres and hemispheres both within a thin dielectric layer as shown in Figures 1 and 2, and at a substrate-air interface. The dipole (i), quadrupole (ii), and octupole (iii) peaks are labelled for the case of the sphere in the film. These geometries were chosen to emulate MNPs that are producible by scalable techniques.[9,28] Comparisons between shapes are difficult for one set of dimensions, as the plasmonic response is due to various aspects of the particle geometry. However, it is possible to observe important traits

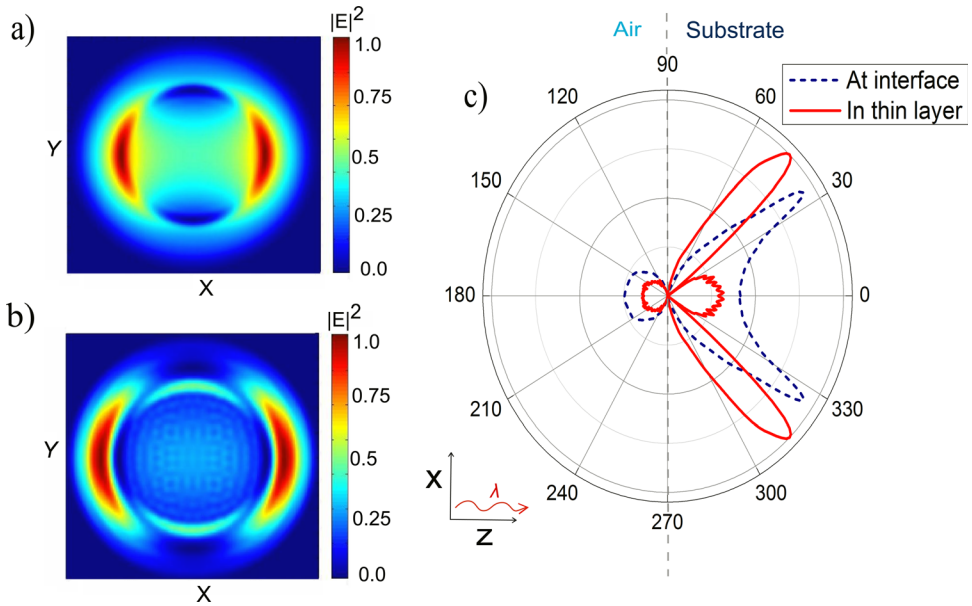

FIG. 3. Simulated far-field emission patterns (a.u.) for a 750 nm dipolar emitter oriented along the *y*-axis. (a) The far-field k-space pattern in the x-y plane for the dipole 75 nm from a substrate-air interface with no film ($n_{film} = 1$). (b) The far field pattern for an identical emitter in the structure proposed in Fig. 1, with $z_- = 75$ nm, $z_+ = 200$ nm, $n_{film} = 1.5$. (c) Angular scattering distribution for both cases measured along the x-axis; showing forward and backwards scattering.

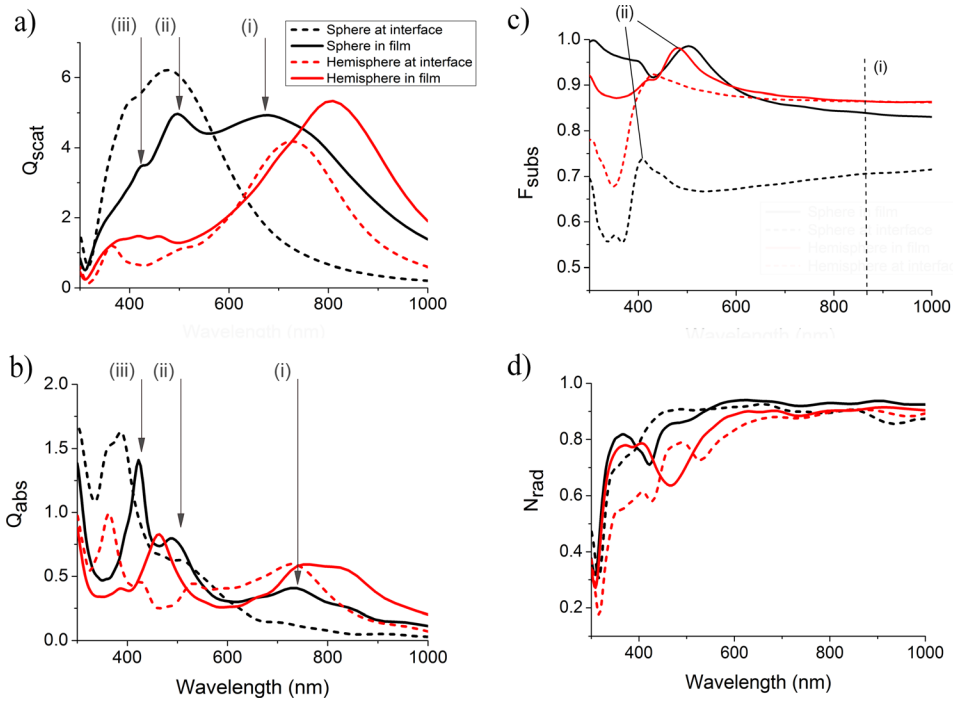

FIG. 4. (a) Scattering and (b) absorption cross sections for 150 nm spheres and hemispheres both at a bare interface (dashed lines) and in the structure defined in Fig. 2 (solid lines) with particles resting on the substrate and the film height above the particle centre (z_+) at 200 nm. The dipole (i), quadrupole (ii), and octupole (iii) peaks are labelled for the case of the sphere in the film. (c) Fraction of radiation scattered forward into the substrate (F_{subs}), also highlighting the dipolar regime (i) and the quadrupole resonance (ii). (d) Radiative efficiency (N_{rad}) of the particles.

of a given geometry that particles of any dimensions will share. Here, we have chosen to equalise the diameters of the particles, which produce results that can be used for a meaningful comparison.

In Fig. 4(a), the addition of the film redshifts and broadens the scattering peaks for both particles—this occurs due to the RI increase in the environment of the MNP, which causes a reduction in the charge separation within the particle, the restoring force, so the resonances occur at longer wavelengths.[2] For spheres, the dipolar peak is shifted by 200 nm from 480 to 680 nm, whilst the quadrupole undergoes a smaller shift of 105 nm from 390 to 495 nm. For the same reason, the primary resonance of the hemispherical MNPs exists at longer λ than that of the sphere, as the geometry results in greater surface contact with the high-index substrate. Since hemispheric MNPs already experience a higher overall dielectric environment compared with spheres, a less dramatic redshift is observed with the addition of the film.

For spheres at an interface, the dipolar mode at 480 nm is the dominant feature and scattering is weak at long wavelengths. With the addition of the film, spheres exhibit a much more broadband response, covering almost the entire spectrum. This is due to both the broadening of the dipolar peak through radiation damping[36] and the higher RI of the film shortening the wavelength of light in the film, giving the particle a larger effective size and leading to the excitation of higher order modes—the quadrupole (ii) at 495 nm and octupole (iii) at 420 nm. Plasmonic modes excited in hemispheres are spatially different to those in spheres due to the large degree of surface contact with the high RI substrate.[37,38] This leads to two different resonances: The primary, long λ mode is excited around the MNP–substrate interface and dominates the spectrum with and without the film. A weaker, secondary mode around 400 nm is also excited about the interface of the MNP with either air or the film material.

Figure 4(b) shows the absorption cross sections (Q_{abs}) of the particles. Each excited mode manifests itself as an absorption peak, with the highest-order mode for each particle having the largest peak value and the dipolar peak the lowest. The addition of the film redshifts all resonances whilst broadening the peak and reducing the maximum value from around 1.6–1.4 for spheres and 1.0–0.8 for hemispheres.

An important parameter is the fraction of the scattered light that can be coupled to the substrate (labelled F_{subs} here). Figure 4(c) compares F_{subs} for spheres and hemispheres both within the film and at a bare interface. At a bare interface, hemispheres exhibit greater forward scattering than spheres due to their increased proximity to the substrate, which produces a strong evanescent coupling.[39] In the layered structure, however, much of the emission from spheres at large angles is caught by the film and reflected forward into the substrate, significantly increasing the forward coupled fraction by a factor of 1.41 overall and a factor of 1.23 in the dipolar region. Coupling for spheres is still inferior in the exclusively dipolar region (i), defined here as 600–1000 nm, by a margin of 2%, since due to their proximity to the substrate, hemispheres achieve very strong coupling at wide angles so the film has a minimal impact on their forward coupling at long wavelengths.

There are several other mechanisms at play here: For particles at an interface, a dramatic drop in forward scattering occurs around the secondary resonance (ii) (the quadrupole for spheres and the MNP-air resonance for hemispheres). This is due to a Fano effect between modes,[40,41] which results in an increase in forward scattering for wavelengths just above the secondary mode and a significant reduction immediately beneath. The addition of the layer around the particle has a drastic effect on this short-wavelength drop in F_{subs} and leads to an extremely high forward coupling where there was

previously a loss. This enhancement in F_{subs} around the Fano peak with the addition of the film leads to greater forward scattering for spheres compared to hemispheres up to around 650 nm.

Figure 4(d) shows the radiative efficiency, N_{rad} of the particles in the two structures, which is a measure of how much of the plasmonic extinction is due to re-emission compared with absorption and is defined as: $N_{rad} = \frac{Q_{scat}}{Q_{scat}+Q_{abs}}$. N_{rad} reveals the minimum overall absorption we can expect from an array of particles,[42] with higher N_{rad} enabling lower absorption if MNPs are optimally spaced. Figure 4(d) shows that except for a dip around 420 and 480 nm due to absorption at high-order resonances, spheres and hemispheres in the layer display a slightly greater radiative efficiency across the solar spectrum than identical particles at a simple interface.

These results demonstrate that by placing a MNP in a thin-film structure, the scattering and absorption resonance peaks can be manipulated and the forward scattering behaviour of higher-order resonances can be altered significantly, leading to a notable reduction in backscatter. As the effect of the film seems to be the most pronounced for spheres, this will be the particle geometry used for subsequent investigations in this paper.

V. EFFECT OF THE REFRACTIVE INDEX OF THE FILM

The RI of each layer will have a large impact on the scattering and will be crucial to determine the optimum location for a MNP within a given multilayered structure. Figure 5 shows the effect of varying the RI of the layer containing a 100 nm Ag sphere between $n_{film} = 1$, the case of a particle at a bare interface, and $n_{film} = 2.2$, a value greater than that of the substrate. In Fig. 5(a), it is clear that raising n_{film} redshifts and broadens all of the particle resonances, but the effect is most pronounced for the dipolar peak, which redshifts almost 400 nm over the range considered and broadens by more than a factor of 4, compared to a 200 nm shift and minimal broadening for the quadrupole mode. This variation in the effect the environment surrounding an MNP has on the different modes has been observed previously for the case of a particle in a uniform dielectric.[42] The presence of this additional layer, therefore, opens up a new mechanism alongside particle geometry to tune the resonance peaks to the desired range of the solar spectrum.

Figure 5(c) shows the fraction of photons scattered into the substrate for various values of film index, n_{film}—it can be seen that increasing n_{film} up to that of the substrate, n_{subs} leads to an increase in the fraction scattered forward across the spectrum up to a factor of 1.3 when $n_{film} = 1.8$. This can be attributed to the increased contrast between the index of the film and the upper half space, leading to stronger reflection from the back face which is then re-scattered in the forward direction. For 150 nm spheres, a maximum enhancement factor of 1.45 was found (not shown), largely due to the increased influence of higher order resonances.

The Fano peak (i) at around 400–600 nm, which was observed earlier in Fig. 4(c), can be seen to redshift in step with the quadrupole peak (ii). When $n_{film} > n_{subs}$, the situation changes somewhat and in the dipolar zone a marked decrease in F_{subs} can be observed. This is due to the fact that some large-angle emission from the dipolar region will now be trapped within the layer via total internal reflection and so will no longer contribute to forward scattering.

Fig. 5(d) shows the far-field scattering pattern along the x-axis at the dipolar peak. As n_{film} is raised, the angle of total internal reflection between the two layers increases and the angle of strongest emission increases in step. The peaks also broaden as the large-angle evanescent contribution gains

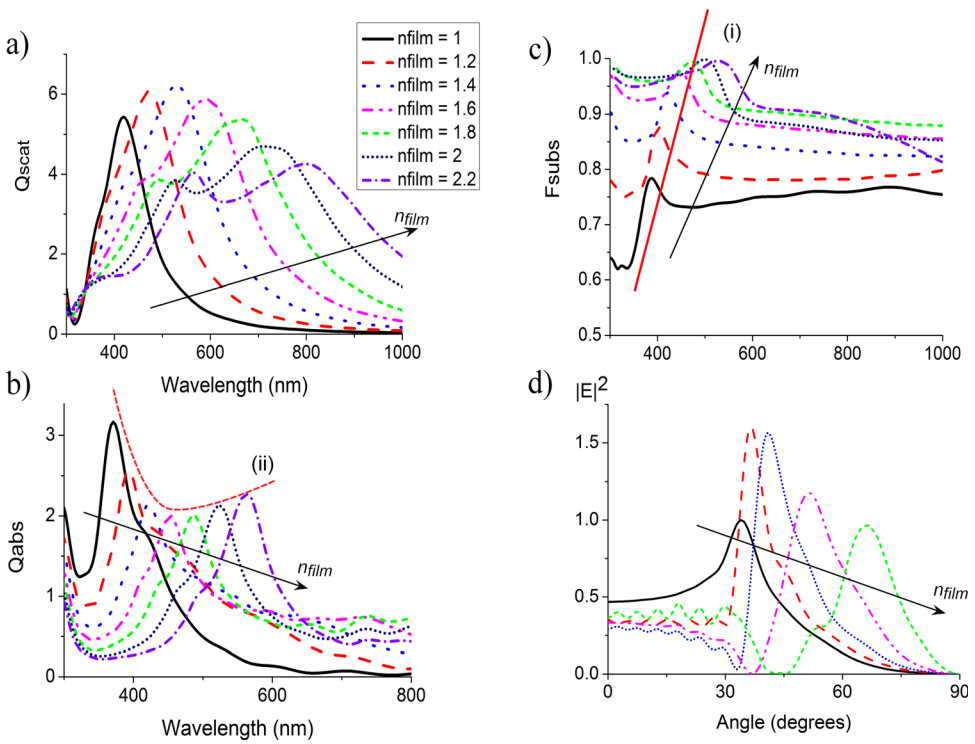

FIG. 5. (a) The scattering cross section, (b) absorption cross section, (c) fraction scattered forward, and (d) angular scattering distribution along the x-axis for 100 nm Ag spheres in the structure defined in Sec. II. The spheres were placed upon the substrate ($z_- = 50$ nm) with $z_+ = 200$ nm, $n_{subs} = 1.8$ and n_{film} varied between 1.0 and 2.2.

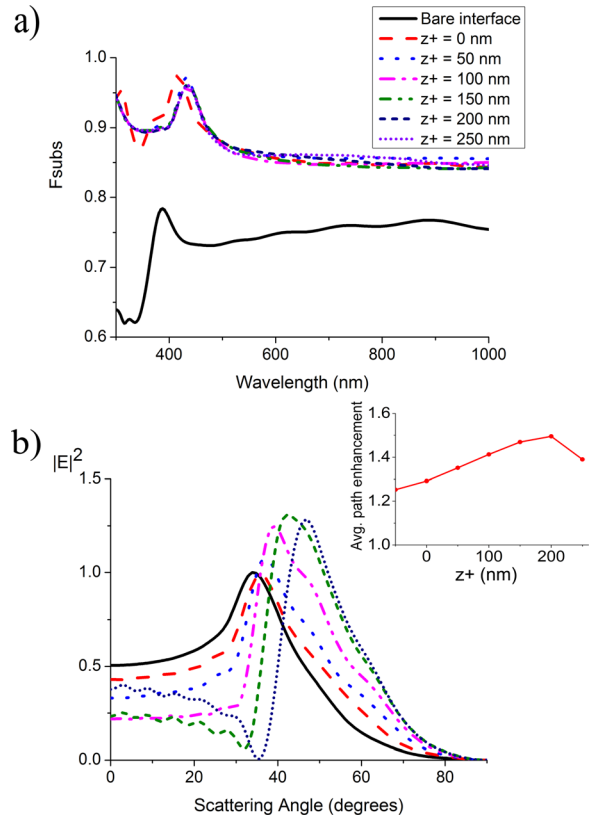

FIG. 6. (a) Fraction scattered forward for different film heights above a 100 nm Ag MNP resting on a substrate with $n_{subs} = 1.8$. (b) Far-field scattering patterns measured perpendicular to the incident polarization for varying z_+. Inset: The average path length enhancement for varying z_+.

significance. When $n_{film} > n_{subs}$, the film behaves like an optical cavity, with the majority of emission very close to the normal, (not shown) leading to a severe reduction of high-angle scattering.

VI. LAYER THICKNESS AND PARTICLE POSITION

As discussed in Sec. III, the properties of an emitter within a thin film depend on both the thickness of the layer and the position of the particle within it. Figure 6(a) shows that by half-covering the particle with the film ($z_- = 50$ nm, $z_+ = 0$ nm) the waveguide behaviour of the film is established and there is a significant increase in the fraction coupled to the substrate. Here, F_{subs} increases by 24% averaged across the entire spectrum and 13% in the dipolar regime alone. Once the particle is covered by the film ($z_+ = 50$ nm), there are minimal further increases in F_{subs}. However, Figure 6(b) shows that there is an effect on the scattering pattern: changing the distance to the back plane will alter the interference effects and dictate the scattering pattern in the substrate, producing a maximum average scattering angle at around $z_+ = 200$ nm.

It has been found by others[15,38] that by altering the thickness of a spacer layer between a MNP and the substrate, and thus the distance to the substrate, an increase in scattering cross section can be achieved. This occurs as the dipolar cross section is defined by the driving field at the particle centre, which is a superposition of the incident field, E_i and that reflected by the interface, E_r. By adding a spacer layer, the phase E_r can be adjusted to minimise destructive interference between E_r and E_i.

Figure 7 shows that an identical effect can be achieved for a particle in a multi-layered structure by changing the distance from the particle center to the substrate, z_-. In Fig. 7(a), the scattering cross section for the dipolar peak can be seen to follow a sinusoidal pattern as the MNP-substrate separation changes the phase of E_r and thus the interference determining the driving field. A maximum Q_{scat} peak value of 7.2 is obtained at $z_- = 85$ nm; a 15% increase from the case where the MNP rests upon the substrate. Figure 7(b) shows that this enhancement is principally related to the dipolar peak and the effect on the quadrupole is far less pronounced.

Figures 7(a-i) and 7(a-ii) show k-space plots displaying how moving the particle away from the substrate modifies the far-field scattering pattern by removing the large-angle evanescent contribution. This can be seen to produce a more well-defined emission pattern in Fig. 7(a-ii), which could be useful for nanoantenna applications.[5,6]

The loss of the evanescent contribution can cause quite severe reductions in the fraction scattered forward as the thickness is increased for particles on a high index substrate. Figure 8 compares F_{subs} for 100 nm spheres in the structure and at an interface. Once again, the effect of the film is very different in the dipolar and quadrupolar regions. As z_- increases, F_{subs} at large wavelengths drops away, as the substrate exerts less of an effect on the particle and so the near-field coupling is reduced. Particles at an air interface show an average reduction in F_{subs} of 5% in the dipolar regime, compared with 2.5% for MNPs in a film. The reduced loss with the film occurs since even with less radiation

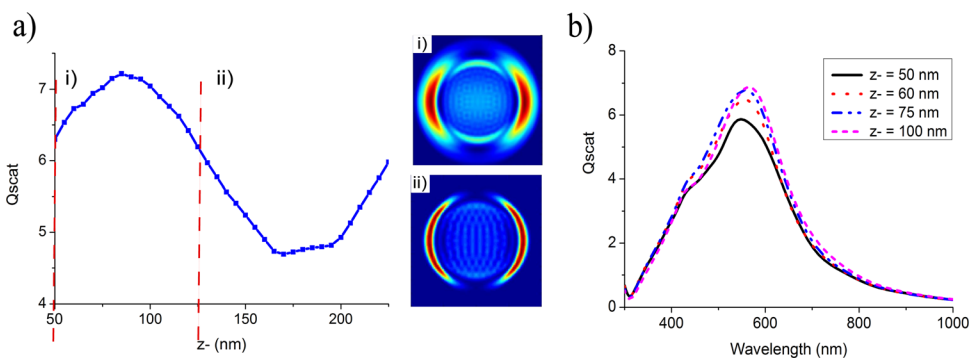

FIG. 7. (a) The scattering cross section at the dipolar peak (560 nm) for a 100 nm Ag sphere with a variable distance between the particle centre and the substrate, z_-. (i) and (ii) k-space plots showing the far-field scattering pattern for the particle at $z_- = 50$ and 125 nm, respectively. (b) The scattering cross section across the solar spectrum with z_- values from 50 to 100 nm showing that the enhancement in Q_{scat} is centred about the dipolar peak. $z_+ = 200$ nm in all cases.

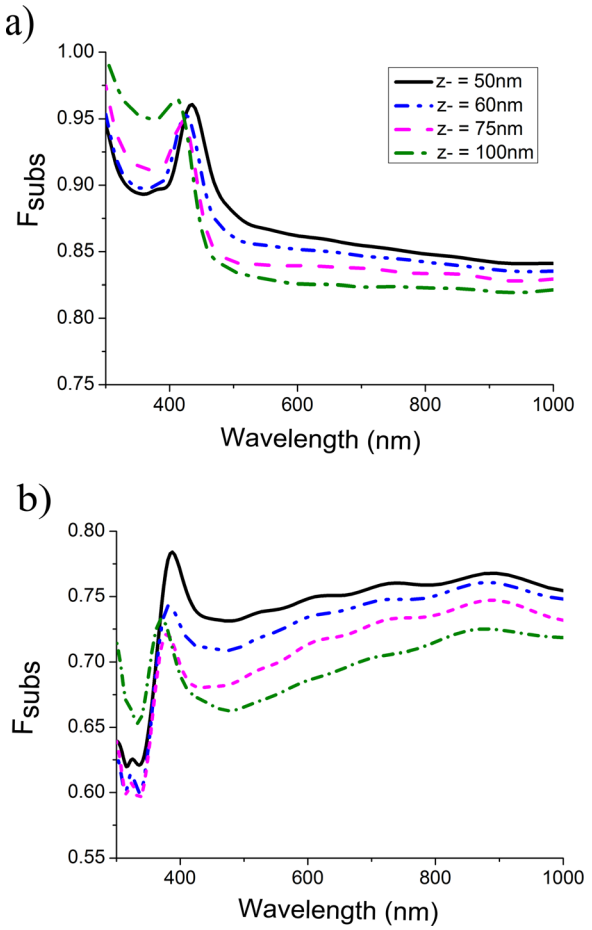

FIG. 8. The fraction of radiation scattered forward (F_{subs}) by 100 nm spheres across the solar spectrum both in a thin film (a) and on the surface of a spacer layer (b) for varying distance from the particle centre to the substrate z_-. $z_+ = 200$ nm in all cases.

emitted directly into the substrate, there will still be a large fraction trapped in the film and reflected forward. Above the quadrupole resonance, for particles in the film there is actually an improvement in forward scattering with increasing z_-. The causes of this increase are not yet understood although it is likely to be related to a complex relationship between quadrupole emission and reflections within the layer.

VII. RELEVANCE TO PV STUDIES

An important application for this study is for use in thin-film solar cells, where the MNPs can act as both an antireflection layer and a light trapping mechanism. Many of the trends observed here contain useful information for maximising the enhancements these particles can bring to PV devices.

In a solar cell, any light scattered away from the substrate will reduce the fraction of light that can be absorbed in the active layer. In Fig. 4(c), we demonstrate that the addition of a thin dielectric film above the particle can reduce backscatter across the solar spectrum. On the other hand, absorption in particles above the active layer in a solar cell will reduce the amount of light available to generate charge carriers. Fig. 4(b) demonstrates that whilst the addition of the film reduces the absorption peak heights, the broadening and red-shifting of resonances, plus the excitation of additional strongly absorbing high-order modes could prove detrimental and would have to be balanced against the possible gains of this structure.

Figure 5 shows how the scattering behaviour can be adjusted by changing the RI of the film. The addition of any layer around the particle with $n_{air} < n_{film} \leq n_{subs}$ will both increase the fraction scattered forward and the optical path length within the substrate. For $n_{subs} = 1.8$, a maximum F_{subs} enhancement of 30%, and a doubling of the average path length in the substrate from normal incidence (a 70% improvement from the case of a particle at a bare interface), was observed when $n_{film} = 1.8$.

It was also seen that placement within a film with a higher RI than the substrate can reduce enhancements. This can be a particular problem in OPV cells, where the obvious location for MNP scatterers is within the PEDOT layer between the active layer and the transparent conducting oxide (TCO) front contact.[43–45] However, across a large portion of the solar spectrum, most commonly used TCOs have a larger RI than P3HT:PCBM[30,46,47] and so losses are observed around the dipolar peak as the particles scatter preferentially into the high-index TCO.

From these figures, it could be assumed that the best location for a particle is within the active layer itself, or at least in a layer with optical properties as close to this as possible. A study by Zhu *et al.*[48] showed that a significant absorption enhancement in the overall structure could be obtained by placing particles in a well defined array at the upper edge of the active layer. However, an inspection of Figure 5(b) reveals that increasing the RI around the particles redshifts the highly absorbing quadrupole resonance and thus extends the strong plasmonic absorption region to longer wavelengths, which could be damaging to the PCE. Wang *et al.*[24] investigated particle position inside the active layer and demonstrated that absorption was minimised in the particle and maximised in the charge-generating medium when MNPs were placed at the bottom of this layer. This solves the problem of particle absorption, but unfortunately MNP placement within the active layer has been shown to enhance recombination in OPV cells, which is detrimental to the cell efficiency.[49] It has also been demonstrated that MNP placement outside the active layer does not have a negative effect on charge transport and can even enhance charge dissociation,[18] highlighting the importance of understanding the effect of the multi-layered structure.

Figures 7 and 8 show that there is also some benefit to altering the position of the particle in the film. Fig. 7 demonstrates that increasing the height of film above the particle can lead to an increase in the average angle over which light is scattered, leading to a maximum average path length enhancement of 50% from the case of a particle at a bare interface. The film will also have some antireflection properties, however, and these would have to be balanced against the potential gains from larger scattering angles. Figure 7 shows that enhancements in Q_{scat} are possible by tuning the distance of the MNP to the substrate, which would allow particles to be spaced further apart and thus reduce absorption. This comes at the cost of a reduction in forward scattering

(although less damaging than for a particle at a bare interface) and in scattering to large angles due to a reduction in near field coupling, which would be detrimental to cell performance.

VIII. CONCLUSIONS

This study has shown that a MNP placed within a thin-film structure displays markedly different scattering properties compared with an identical particle at a simple interface. This can be partially explained by a simple dipolar model, but is also seen to depend strongly on the interaction of the MNP with the surrounding environment, which dictates the resonance conditions for the excited plasmonic modes.

The addition of a dielectric film around a MNP at an interface with $n_{air} < n_{film} < n_{subs}$ was seen to enhance the fraction of light scattered into the substrate across the solar spectrum, both through the coupling of large-angle emission into the quasi-waveguide modes of the layer, which are then scattered forward, and by reducing back-scatter due to a Fano resonance about the secondary mode. It was found that films with RI values not conforming to $n_{air} < n_{film} < n_{subs}$ could show a reduction in F_{subs} in the dipolar regime, highlighting the importance of placing plasmonic scatterers in a region where these conditions can be fulfilled. The high refractive index of most common TCOs can make this difficult in OPV cells.

There are many potential benefits for solar cells via tailoring the photonic layers around a plasmonic scatterer which have been demonstrated, such as additional tunability of resonances, increased forward scattering, and optical path length enhancement. This can come at the cost of greater parasitic MNP absorption at long wavelengths, however, and so an optimisation of the parameters described would need to be conducted for any given cell structure. Some control over the emission pattern has been achieved through adjusting the properties of the film, which could be of interest for nanoantenna research.

ACKNOWLEDGMENTS

This work was supported by the UK Engineering and Physical Sciences Research Council. J.M.S. acknowledges additional support from Hewlett Packard Ltd.

[1]J. Heber, "Surfing the wave," Nature **461**, 720–722 (2009).
[2]M. Garcia, "Surface plasmons in metallic nanoparticles: Fundamentals and applications," J. Phys. D **44**, 283001 (2011).
[3]J. N. Anker, W. P. Hall, O. Lyandres, N. C. Shah, J. Zhao, and R. P. Van Duyne, "Biosensing with plasmonic nanosensors," Nature Mater. **7**, 442 (2008).
[4]H. Atwater and P. Polman, "Plasmonics for improved photovoltaic devices," Nature Mater. **9**, 205–213 (2010).
[5]T. H. Taminiau, F. D. Stefani, F. B. Segerink, and N. F. van Hulst, "Optical antennas direct single-molecule emission," Nature Photon. **2**, 234–237 (2008).
[6]A. G. Curto, G. Volpe, T. H. Taminiau, M. P. Kreuzer, R. Quidant, and N. F. van Hulst, "Unidirectional emission of a quantum dot coupled to a nanoantenna," Science **329**(5994), 930–933 (2010).
[7]R. S. Pavlov, A. G. Curto, and N. F. Van Hulst, "Log-periodic optical antennas with broadband directivity," Opt. Commun. **285**(16), 3334–3340 (2012).
[8]J. Nelson, *The Physics of Solar Cells* (Imperial College Press, 2003).
[9]S. Pillai, K. Cathpole, T. Trupke, and M. A. Green, "Surface plasmon enhanced solar cells," J. Appl. Phys. **101**, 093105 (2007).
[10]W. Ren, G. Zhang, Y. Wu, H. Ding, Q. Shen, K. Zhang, J. Li, N. Pan, and X. Wang, "Broadband absorption enhancement achieved by optical layer mediated plasmonic solar cell," Opt. Express **19**, 26536 (2011).
[11]A. Ji, Sangita, and R. P. Sharma, "A study of nanoellipsoids for thin-film plasmonic solar cell applications," J. Phys. D: Appl. Phys. **45**, 275101 (2012).
[12]T. Temple, G. Mahanama, H. Reehal, and D. Bagnall, "Influence of localized surface plasmon excitation in silver nanoparticles on the performance of silicon solar cells," Sol. Energy Mater. Sol. Cells **93**, 1978–1985 (2009).
[13]A. Basch, F. Beck, T. Soderstrom, S. Varlamov, and K. Catchpole, "Combined plasmonic and dielectric rear reflectors for enhanced photocurrent in solar cells," Appl. Phys. Lett. **100**, 243903 (2012).
[14]F. J. Beck, A. Polman, and K. R. Catchpole, "Tunable light trapping for solar cells using localized surface plasmons," J. Appl. Phys. **105**, 114310 (2009).
[15]F. J. Beck, S. Mokkapati, A. Polman, and K. R. Catchpole, "Asymmetry in photocurrent enhancement by plasmonic nanoparticle arrays located on the front or on the rear of solar cells," Appl. Phys. Lett. **96**, 033113 (2010).
[16]S. Pillai, F. J. Beck, K. R. Catchpole, Z. Ouyang, and M. A. Green, "The effect of dielectric spacer thickness on surface plasmon enhanced solar cells for front and rear side depositions," J. Appl. Phys. **109**, 073105 (2011).
[17]X. Chen, B. Jia, J. K. Saha, B. Cai, N. Stokes, Q. Qiao, Y. Wang, Z. Shi, and M. Gu, "Broadband enhancement in thin-film amorphous silicon solar cells enabled by nucleated silver nanoparticles," Nano Lett. **12**(5), 2187–2192 (2012).
[18]J. L. Wu, F.-C. Chen, Y.-S. Hsiao, F.-C. Chien, P. Chen, C.-H. Kuo, M. H. Huang, and C.-S. Hsu, "Surface plasmonic effects of metallic nanoparticles on the performance of polymer bulk heterojunction solar cells," ACS Nano **5**(2), 959–967 (2011).
[19]G. Mie, "Contributions to the optics of turgid media, particularly solutions of colloidal metals," Ann. Phys. **25**, 377 (1908).
[20]K. L. Kelly, E. Coronado, L. L. Zhao, and G. C. Schatz, "The optical properties of metal nanoparticles—The influence of size, shape, and dielectric environment," J. Phys. Chem. B **107**, 668–677 (2003).
[21]W. S. Wong and A. Salleo, *Flexible Electronics: Materials and Applications* (Springer, 2009).
[22]R. S. Sesuraj, T. Temple, and D. M. Bagnall, "Tunable low-loss plasmonic mirror for diffuse optical scattering," Appl. Phys. Express **5**, 125205 (2012).
[23]R. Sesuraj, T. Temple, and D. Bagnall, "Optical characterisation of a spectrally tunable plasmonic reflector for application in thin-film silicon solar cells," Sol. Energy Mater. Sol. Cells **111**, 23–30 (2013).
[24]S.-Y. Wang, D.-A. Borca-Tasciuc, and D. A. Kaminski, "The effect of particle vertical positioning on the absorption enhancement in plasmonic organic solar cells," J. Appl. Phys. **111**(12), 124301 (2012).
[25]J. A. Töfflinger, E. Pedrueza, V. Chirvony, C. Leendertz, R. García-Calzada, R. Abargues, O. Gref, M. Roczen, L. Korte, J. P. Martínez-Pastor, and B. Rech, "Photoconductivity and optical properties of silicon coated by thin tio2 film in situ doped by au nanoparticles," Phys. Status Solidi A **210**, 687 (2013).
[26]K. G. Lee, X. W. Chen, H. Eghlidi, P. Kukura, R. Lettow, A. Renn, and V. S. S. Gtzinger, "A planar dielectric antenna for directional single-photon emission and near-unity collection efficiency," Nature Photon. **5**, 166–169 (2011).
[27]L. Luan, P. R. Sievert, W. Mu, Z. Hong, and J. B. Ketterson, "Highly directional fluorescence emission from dye molecules embedded in a dielectric layer adjacent to a silver film," New J. Phys. **10**, 073012 (2008).
[28]D. D. Evanoff and G. Chumanov, "Synthesis and optical properties of silver nanoparticles and arrays," Chemphyschem **6**, 1221–1231 (2005).
[29]P. Spinelli, C. van Lare, E. Verhagen, and A. Polman, "Controlling fano lineshapes in plasmon-mediated light coupling into a substrate," Opt. Express **19**, A303–A311 (2011).
[30]F. Monestier, J.-J. Simona, P. Torchioa, L. Escoubasa, F. Florya, S. Bailly, R. de Bettignies, S. Guillerez, and C. Defranoux, "Modeling the short-circuit current density of polymer solar cells based on P3HT:PCBM blend," Sol. Energy Mater. Sol. Cells **91**, 405–410 (2007).
[31]H. Hoppe, N. S. Sariciftci, and D. Meissner, "Optical constants of conjugated polymer/fullerene based bulk-heterojunction organic solar cells," Mol. Cryst. Liq. Cryst. **385**, 113 (2002).

[32]See http://www.lumerical.com/ for "Lumerical solutions inc."
[33]See http://docs.lumerical.com/en/fdtd/user_guide_tfsf_sources.html for "TFSF sources—FDTD Solutions Knowledge Base."
[34]K. A. Neyts, "Simulation of light emission from thin-film microcavities," J. Opt. Soc. Am. **15**(4), 962 (1998).
[35]J. D. Jackson, *Classical Electrodynamics*, 3rd ed. (Wiley, 1999).
[36]M. Meier and A. Wokaun, "Enhanced fields on large metal particles: Dynamic depolarization," Opt. Lett. **8**, 581–583 (1983).
[37]C. Hägglund, M. Zäch, G. Petersson, and B. Kasemo, "Electromagnetic coupling of light into a silicon solar cell by nanodisk plasmons," Appl. Phys. Lett. **92**, 053110 (2008).
[38]F. J. Beck, E. Verhagen, S. Mokkapati, A. Polman, and K. R. Catchpole, "Resonant SPP modes supported by discrete metal nanoparticles on high-index substrates," Opt. Express **19**(Suppl. 2), A146 (2011).
[39]K. Catchpole and A. Polman, "Plasmonic solar cells," Opt. Express **16**(26), 21793 (2008).
[40]S. H. Lim, W. Mar, P. Matheu, D. Derkacs, and E. T. Yu, "Photocurrent spectroscopy of optical absorption enhancement in silicon photodiodes via scattering from surface plasmon polaritons in gold nanoparticles," J. Appl. Phys. **101**(10), 104309 (2007).
[41]B. Luk'yanchuk, N. I. Zheludev, S. A. Maier, N. J. Halas, P. Nordlander, H. Giessen, and C. T. Chong, "The fano resonance in plasmonic nanostructures and metamaterials," Nature Mater. **9**, 707–715 (2010).
[42]T. L. Temple and D. M. Bagnall, "Broadband scattering of the solar spectrum by spherical metal nanoparticles," Prog. Photovoltaics (to be published).
[43]I. Diukman, L. Tzabari, N. Berkovitch, N. Tessler, and M. Orenstein, "Controlling absorption enhancement in organic photovoltaic cells by patterning au nano disks within the active layer," Opt. Express **19**(S1), A64 (2011).
[44]I. Kim, T. S. Lee, D. S. Jeong, W. S. Lee, and K.-S. Lee, "Size effects of metal nanoparticles embedded in a buffer layer of organic photovoltaics on plasmonic absorption enhancement," J. Phys. D: Appl. Phys. **45**, 065101 (2012).
[45]B. Wu, X. Liu, T. Z. Oo, G. Xing, N. Mathews, and T. C. Sum, "Resonant aluminum nanodisk array for enhanced tunable broadband light trapping in ultrathin bulk heterojunction organic photovoltaic devices," Plasmonics **7**, 677 (2012).
[46]E. Palik, *Handbook of Optical Constants of Solids* (Academic, New York, 1998).
[47]K. Ding, T. Kirchartz, B. E. Pieters, C. Ulbrich, A. M. Ermes, S. Schicho, A. Lambertz, R. Carius, and U. Rau, "Characterization and simulation of a-si:h/c-si:h tandem solar cells," Sol. Energy Mater. Sol. Cells **95**(12), 3318–3327 (2011).
[48]J. Zhu, M. Xue, H. Shen, Z. Wu, S. Kim, J.-J. Ho, A. Hassani-Afshar, B. Zeng, and K. L. Wang, "Plasmonic effects for light concentration in organic photovoltaic thin films induced by hexagonal periodic metallic nanospheres," Appl. Phys. Lett. **98**(15), 151110 (2011).
[49]M. Xue, L. Li, B. J. T. de Villers, H. Shen, J. Zhu, Z. Yu, A. Z. Stieg, Q. Pei, B. J. Schwartz, and K. L. Wang, "Charge-carrier dynamics in hybrid plasmonic organic solar cells with ag nanoparticles," Appl. Phys. Lett. **98**(25), 253302 (2011).